

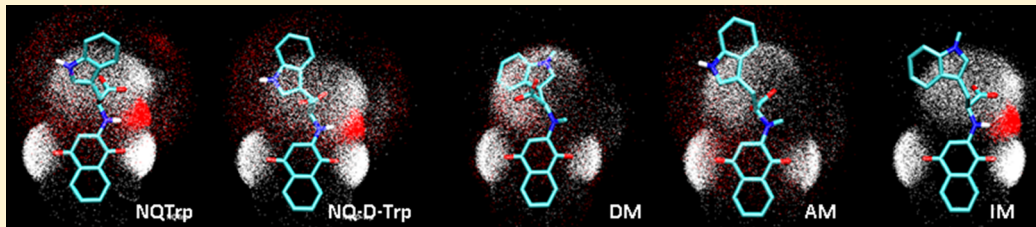
# Methylations of Tryptophan-Modified Naphthoquinone Affect Its Inhibitory Potential toward $\text{A}\beta$ Aggregation

Roni Scherzer-Attali,<sup>†,‡</sup> Marino Convertino,<sup>†,§</sup> Riccardo Pellarin,<sup>§</sup> Ehud Gazit,<sup>\*,‡</sup> Daniel Segal,<sup>\*,‡,||</sup> and Amedeo Caflisch<sup>\*,§</sup>

<sup>†</sup>Department of Molecular Microbiology and Biotechnology and <sup>||</sup>Sagol School of Neurosciences, Tel-Aviv University, Tel-Aviv 69978, Israel

<sup>§</sup>Department of Biochemistry, University of Zurich, Winterthurerstrasse 190, CH-8057 Zurich, Switzerland

## Supporting Information



**ABSTRACT:** Aggregation of amyloid beta ( $\text{A}\beta$ ) is the hallmark of Alzheimer's disease (AD). Small molecules inhibiting  $\text{A}\beta$  can be valuable therapeutics for AD. We have previously reported that 1,4-naphthoquinon-2-yl-L-tryptophan (NQTrp), reduces aggregation and oligomerization of  $\text{A}\beta$  in vitro and in vivo. In silico analysis further showed that certain functional groups of NQTrp, not in the aromatic rings, are also involved in binding and inhibiting  $\text{A}\beta$ . To better understand the exact mode of action and identify the groups crucial for NQTrp inhibitory activity, we conducted structure–activity analysis. Four derivatives of NQTrp were studied in silico: a D-isomer, two single-methylated and one double-methylated derivative. In silico results showed that the NQTrp groups involved in hydrogen bonds are the anilinic NH (i.e., the NH linker between the quinone and tryptophan moieties), the quinonic carbonyls, and the carboxylic acid. These predictions were supported by in vitro results. Our results should aid in designing improved small-molecule inhibitors of  $\text{A}\beta$  aggregation for treating AD.

## INTRODUCTION

Alzheimer's disease (AD), a progressive neurodegenerative disorder for which there is no cure or effective treatment, is the leading cause of dementia in aged humans. AD has been estimated to affect 35.6 million people, around 0.5% of the global population in 2010. By 2050, prevalence will quadruple by which time 1 in 85 persons worldwide will be living with the disease.<sup>1</sup> Strong genetic, physiological and biochemical evidence suggests that the 42-residue amyloidogenic peptide amyloid beta ( $\text{A}\beta$ ) plays a key role in the pathogenesis of the disease.<sup>2</sup> Although the etiologic role of  $\text{A}\beta$  in AD is acknowledged,<sup>3</sup> the molecular mechanism of its neurotoxicity is still under debate. The major neuropathological changes in the brains of AD patients include neuronal death, particularly in regions related to memory and cognition and the presence of intra- and extracellular abnormal protein aggregates<sup>4,5</sup> known as amyloid plaques, composed of  $\text{A}\beta$ , neurofibrillary tangles, containing the tau protein, respectively. The  $\text{A}\beta$  peptide is intrinsically disordered as it populates various conformations in solution. Due to its unstructured nature and its high propensity to aggregate, it cannot be crystallized. The two major versions of  $\text{A}\beta$  are 40 and 42 residues long ( $\text{A}\beta_{1-40}$  and  $\text{A}\beta_{1-42}$ , respectively), which differ in the absence or presence of two extra C-terminal residues. Both versions can form amyloid

fibrils in vitro that are very similar to those found in the brains of AD patients. Accumulating evidence indicates a fundamental role of the early soluble oligomeric species of  $\text{A}\beta$ , rather than the mature fibrillar species, in the pathogenesis of AD.<sup>6–10</sup>

Our group and others have previously identified the key role of aromatic amino acids in the formation of amyloid fibrils through  $\pi$ -stacking interactions.<sup>11–18</sup> We speculated that stacking interactions rather than mere hydrophobic interactions may provide an energetic contribution as well as order and directionality to the self-assembly of amyloid structures. This hypothesis has recently gained direct evidence by high-resolution structural studies by other researchers, who also suggested that aromatic interactions could be a target for antiamyloid therapy.<sup>19,20</sup> The stacking hypothesis suggests a new approach to understand the self-assembly mechanism that governs amyloid formation, enables the identification of novel motifs, and indicates possible ways to control this process.

Various strategies have been attempted to date for inhibiting both oligomers and amyloid formation of the  $\text{A}\beta$  peptide. One approach that gained attention in recent years is the use of

Received: September 12, 2012

Revised: December 23, 2012

Published: December 23, 2012

Table 1. NQTrp and Its Derivatives Used in This Study

Derivative	Simulation Name	Structure	Comments
1,4-naphthoquinone-2-yl-L-tryptophan	NQTrp		
1,4-naphthoquinone-2-yl-D-tryptophan	NQ-D-Trp		The stereochemistry is inverted
N-methylamino-NQTrp	AM		NQTrp derivative bearing the anilinic methylated nitrogen
N-methylindol-NQTrp	IM		NQTrp derivative bearing the indolic methylated nitrogen
N,N-dimethyl-NQTrp	DM		NQTrp derivative bearing two methylated nitrogens

small molecules as inhibitors of amyloid formation.<sup>21,22</sup> A major advantage of this approach is that small molecules are good candidates for developing drugs; they can be administrated orally, can penetrate cell membranes, and pass through the blood–brain barrier relatively easily. Early findings demonstrated that small aromatic molecules such as Congo red interact with amyloid fibrils and can inhibit their formation.<sup>23–25</sup> Since then, dozens of small aromatic molecules were shown to inhibit the process of amyloid fibril formation *in vitro*, and in some cases, they were also shown to have a protective effect in cell culture assays (reviewed by Porat et al.<sup>21</sup>). A very interesting property of this large group of small molecules inhibitors is their aromatic nature. Furthermore, a few of these small aromatic molecules were tested with several amyloidogenic proteins and were shown to be generic inhibitors of amyloid fibril formation.<sup>26</sup>

We have previously reported that a small naphthoquinone–tryptophan hybrid molecule, termed NQTrp (Table 1), is a potent inhibitor of both  $A\beta$  amyloid and oligomer formation *in vitro* as well as in an AD fly model.<sup>27</sup> Also, this compound has been shown to be the best binder of  $A\beta$  among several potent inhibitors analyzed using molecular dynamics.<sup>28,29</sup> Using *in silico* analysis,<sup>27</sup> we showed that specific atoms in the NQTrp molecule as well as its aromatic moieties are essential for the

binding to  $A\beta$  and for inhibiting its aggregation. Furthermore, hydrogen bonds were found to be crucial for binding and inhibition of  $A\beta$ . Specifically, the most frequent hydrogen bonds of NQTrp with the peptide backbone of  $A\beta$  include NH1-CO, CO1-NH, and CO3-NH (NH1 corresponds to the NH linker between the quinone and tryptophan of NQTrp, and CO1 and CO3 correspond to the quinonic carbonyl and the carboxylic acid of Trp, respectively (Table 1)). We also found that the hydrogen bond pairs NH1-CO and CO1-NH or NH1-CO and CO3-NH occur simultaneously at high probability. The *in silico* analysis showed that for oligomer inhibition only the NH linker and carbonyl groups are essential, whereas the indolic NH of the compound is less crucial.

As a result of this conclusion and for further structure activity relations (SAR) analysis, three derivatives of NQTrp were synthesized (Table 1). The first is NQTrp methylated at the NH1 position (hereafter termed AM). The second is NQTrp methylated at the indolic NH position (termed IM), and the third is NQTrp in which the tryptophan is in a D conformation (termed NQ-D-Trp). Synthesis of a fourth molecule in which both NH bonds of NQTrp are methylated (termed DM) was attempted, but due to the unstable nature of the compound, we were not able to retrieve the compound. The goal was to assess whether or not the NH1 position and/or the indolic NH

Table 2. Simulation Results<sup>a</sup>

	$\text{A}\beta_{14-20}$			$\text{A}\beta_{16-22}$			$\text{A}\beta_{18-24}$		
	<i>r</i>	interstrand H bonds	intrastrand H bonds	<i>r</i>	interstrand H bonds	intrastrand H bonds	<i>r</i>	interstrand H bonds	intrastrand H bonds
free	10.20	8.5 ± 0.3	0.10 ± 0.1	1.63	7.1 ± 0.2	0.10 ± 0.10	1.01	6.9 ± 0.3	0.8 ± 0.2
NQTrp	1.88	6.7 ± 0.3	0.58 ± 0.04	0.59	5.0 ± 0.3	0.97 ± 0.03	0.24	4.0 ± 0.3	2.4 ± 0.05
NQ-D-Trp	1.66	6.24 ± 0.1	0.61 ± 0.1	0.55	4.9 ± 0.36	0.99 ± 0.04	0.27	4.29 ± 0.53	2.42 ± 0.14
DM	2.48	6.98 ± 0.7	0.58 ± 0.06	0.73	5.31 ± 0.41	1.02 ± 0.06	0.30	4.51 ± 0.49	2.48 ± 0.1
AM	2.14	6.74 ± 0.65	0.60 ± 0.06	0.66	5.20 ± 0.41	1.00 ± 0.05	0.28	4.37 ± 0.3	2.52 ± 0.07
IM	1.98	6.62 ± 0.7	0.58 ± 0.06	0.58	4.88 ± 0.36	1.01 ± 0.06	0.22	3.98 ± 0.32	2.45 ± 0.06

<sup>a</sup>The order-disorder ratio *r* was calculated using the order parameter  $P_2$ , as explained in the Materials and Methods. The interstrand and intrastrand hydrogen bond values were evaluated for individual peptides and averaged over the three copies of the peptide. All data are averaged over all of the respective MD sampling.

position are essential for NQTrp to bind and inhibit  $\text{A}\beta$ , other than the aromatic rings which were also shown to be crucial. The *D* conformer was synthesized in order to examine if the configuration of the tryptophan (Trp) is also important and if the increased metabolic stability (resistance to proteolysis) conferred by the *D* conformation of Trp will increase its efficacy in binding/inhibiting  $\text{A}\beta$  (Table 1). The effect of the different substitutions and conformation rearrangements on the binding and inhibition of  $\text{A}\beta$  was assessed in silico by molecular dynamics (MD) as well as using various in vitro assays. The results of the two approaches were compared.

## MATERIALS AND METHODS

**Synthesis of Compounds.** *D*-NQTrp. *D*-1,4-naphthoquinon-2-yl-L-tryptophan (NQTrp) was synthesized from *D*-tryptophan and 1,4-naphthoquinone by a one-step synthesis according to the protocol by Shrestha-Dawadi et al.<sup>39</sup> <sup>1</sup>H NMR (DMSO-*d*<sub>6</sub>): δ 3.3 (m, CH<sub>2</sub>), 3.9 (m, CH<sub>2</sub>), 5.6 (s, 1H), 6.8 (t, *J* = 3.3 Hz, 1H), 6.8 (t, *J* = 7.4 Hz, 1H), 7.1 (s, 1H), 7.2 (br m, NH), 7.3 (d, *J* = 8.0 Hz, 1H), 7.4 (d, *J* = 7.5 Hz, 1H), 7.6–7.9 (m, 4H), 10.8 (NH). Reverse phase HPLC showed >95% purity. HR-MS: *m/z* (MH<sup>+</sup>) 361 calcd for C<sub>21</sub>H<sub>18</sub>N<sub>2</sub>O<sub>4</sub>.

*IM-NQTrp*. This was synthesized as NQTrp, but using 1-methyl-indole as starting material. <sup>1</sup>H NMR (DMSO-*d*<sub>6</sub>): δ 3.3 (m, CH<sub>2</sub>), 3.668 (t, CH<sub>3</sub> on indole ring), 3.9 (m, CH<sub>2</sub>), 5.6 (s, 1H), 6.8 (t, *J* = 3.3 Hz, 1H), 6.8 (t, *J* = 7.4 Hz, 1H), 7.1 (s, 1H), 7.2 (br m, NH), 7.3 (d, *J* = 8.0 Hz, 1H), 7.4 (d, *J* = 7.5 Hz, 1H), 7.6–7.9 (m, 4H). Reverse phase HPLC showed >95% purity. HR-MS: *m/z* 375 calcd for C<sub>22</sub>H<sub>18</sub>N<sub>2</sub>O<sub>4</sub>.

*AM-NQTrp*. To synthesize the AM compound, 1 g of NQTrp was synthesized as described by Shrestha-Dawadi et al.<sup>39</sup> The amide NH of NQTrp was methylated using chloromethyldimethylsilyl chloride in the presence of hexamethyldisilazane followed by treatment with cesium fluoride in 2-methoxyethyl ether as in ref 40. Because the product is oxygen sensitive, the reactions were done under Ar and N<sub>2</sub>. The NMR spectrum of the compound was unresolved, though a singlet peak at 10.275 (s, 3H) was clearly seen, which belongs to the methyl on the NH group. It is possible that the conformation of the compounds and the hydrogen anisotropy affect the NMR spectrum, therefore, resulting in an unresolved spectrum. Reverse phase HPLC showed >95% purity. HR-MS: *m/z* calcd 413 (M<sup>+</sup> + K), 242 (quinone-N (CH<sub>3</sub>)-COO<sup>-</sup>), 186 (quinone-N-CH<sub>3</sub>).

**Simulation Protocol.** Molecular dynamics simulations are used to investigate the aggregation of three replicas of  $\text{A}\beta_{14-20}$ ,  $\text{A}\beta_{16-22}$  or  $\text{A}\beta_{18-24}$  in presence or absence of one single NQTrp and analogue (see Table 1) molecules. The simulations were performed with the CHARMM program,<sup>41</sup> the peptide and compounds were modeled using the united atoms CHARMM PARAM19 force field with its default truncation scheme for nonbonding interaction (cutoff of 7.5). Hydration effects were accounted for by using SASA, a solvent-accessible surface based implicit model.<sup>42</sup> NQTrp and its derivative are parametrized as described in ref 27. Bending as well as van der Waals parameters and partial charges for the additional methyl group were

derived from the Cβ atom of alanine in PARAM19. The simulations were prepared by initially placing three monodispersed replicas of the same heptapeptide with or without the presence of a single NQTrp molecule (or its derivatives) in the simulation box. Therefore, the concentration ratio peptide: compound is 3:1. Simulations were carried out with periodic boundary conditions at fixed peptide concentration of 4.88 mM (the simulation boxes were set to 98 Å for  $\text{A}\beta_{14-20}$ , to 96 Å for  $\text{A}\beta_{16-22}$ , to 95 Å for  $\text{A}\beta_{18-24}$ ) using Langevin integrator at low friction constant (0.15 ps<sup>-1</sup>) and at a temperature of 330 K, which yields reversible aggregation within a reasonable computational time. After 100 ns of initial equilibration, a total of 10 2.5 μs independent simulations were run for each system. A 2.5 μs run takes about three weeks on a single AMD Opteron 252 CPU at 2.6 GHz.

**Analysis of Trajectories.** The nematic order parameter  $P_2$  allows one to measure the amount of ordered β-structure in the system.

$$P_2 = \frac{1}{N} \sum_{i=1}^N \frac{3}{2} (\hat{\mathbf{z}}_i \cdot \hat{\mathbf{d}})^2 - \frac{1}{2}$$

where the unit vector  $\mathbf{d}$ , that defines a preferential direction, is the eigenvector of the order matrix that corresponds to the largest positive eigenvalue; the *N* molecular unit vectors  $\mathbf{z}_i$  are built joining the Cα atom of residue *i* to the Cα atom of residue *i* + 2. The values of  $P_2$  range from 0 to 1, which correspond to complete disorder and complete order, respectively. The complete order is achieved when all the unit vectors are parallel or antiparallel, while the disorder is obtained when none of unit vectors is parallel to any of the others. The threshold  $P_2^*$  is a value of the order parameter chosen such that it separates the ordered from the disordered phase and was chosen as  $P_2^* = 0.665$ , as reported previously.<sup>35</sup> To quantify the amount of ordered aggregates, the order-disorder ratio *r* is defined by the number of snapshots where the system has a  $P_2$  value larger than  $P_2^*$  (order) divided by the number of snapshots with  $P_2$  lower than  $P_2^*$  (disorder)

$$r = \frac{n(P_2 > P_2^*)}{n(P_2 < P_2^*)}$$

Another quantitative estimate of the influence of the compounds on the ordered aggregation of the heptapeptides is the interpeptide interaction energy, which is the CHARMM nonbonded energy (van der Waals plus electrostatics) of a single peptide with the other two, without considering the inhibitor. These two measures (the order-disorder ratio and average interpeptide interaction energy) are calculated using only the coordinates of the heptapeptides, irrespective of the type of compound, which allows to directly compare the effect of different compounds.

The average values (Table 2) and time series of HBs (Figure S3 in Supporting Information) were also computed. The HBs are calculated by using a distance threshold of 2.5 Å for the H–O distance and cutoff of larger than 130° for the NH–O angle. It is important to note that these results were obtained from a statistically converged sampling (Figures S1 and S3 in Supporting Information).

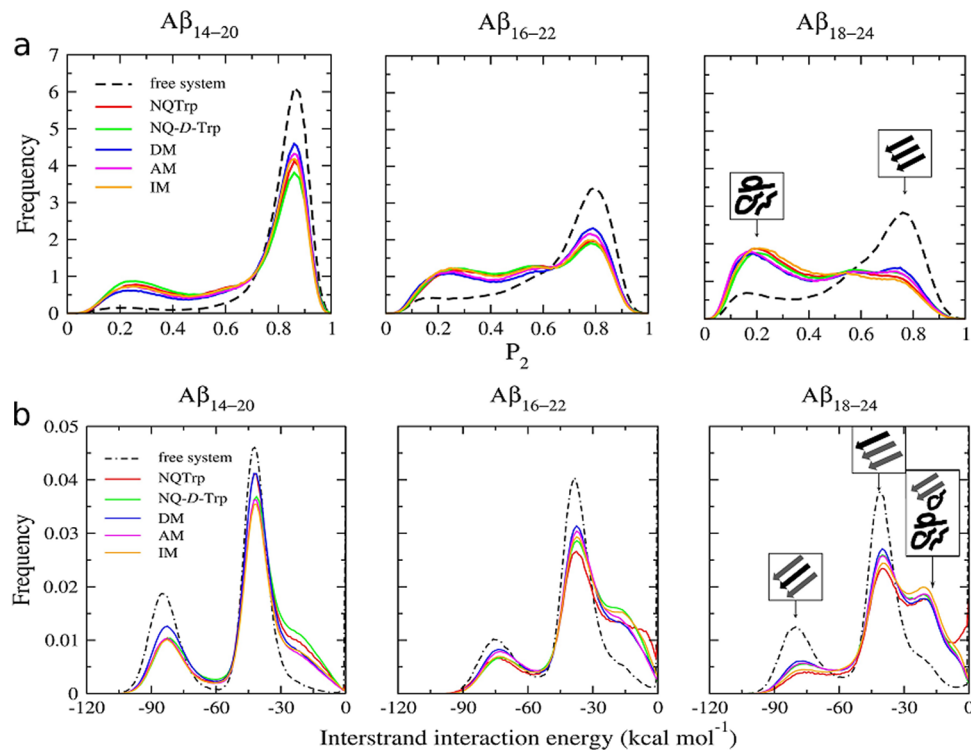


**Figure 1.** (a) Frequency histograms. Frequency histograms of the nematic order parameter  $P_2$  for the three investigated  $\text{A}\beta$  segments. Values of  $P_2$  close to 0.2 and 0.8 correspond to disordered conformations and  $\beta$ -sheet structures, respectively. (b) Interpeptide interaction energy distributions. The two peaks of the distributions of interpeptide interaction energy (see main text) correspond to a peptide in the center of an ordered oligomer (about  $-80$  kcal/mol) and a peptide at the edge of an ordered oligomer (about  $-40$  kcal/mol). The shoulder of the energy distribution at the values of about  $-20$  kcal/mol contains events with disordered or partially ordered oligomers. All of the calculated properties are averaged over a total sampling of  $25\ \mu\text{s}$  (10 independent  $2.5\ \mu\text{s}$  simulations) for each system.

**Determination of Soluble Oligomer Formation.**  $\text{A}\beta$  intermediates and toxic oligomers were produced according to Barghorn and co-workers.<sup>10</sup> To avoid preaggregation, synthetic lyophilized  $\text{A}\beta_{1-42}$  was pretreated with HFIP.  $\text{A}\beta_{1-42}$  was dissolved in 100% HFIP, sonicated for 20 s and incubated for 2 h at  $37^\circ\text{C}$  under shaking at 100 rpm. The appropriate molecule was dissolved in DMSO to a concentration of 30 mM, sonicated for 1 min, and then diluted with DMSO to its final concentrations. After evaporation in a speedVac,  $\text{A}\beta_{1-42}$  was resuspended in DMSO (with or without the appropriate inhibitor) to 5 mM and diluted with 20 mM  $\text{NaH}_2\text{PO}_4$ , 140 mM NaCl, pH 7.4, to a final concentration of 400  $\mu\text{M}$  and 1/10 volume 2% SDS (final concentration of 0.2%). The toxic  $\text{A}\beta$  oligomers were generated by further dilution with two volumes of  $\text{H}_2\text{O}$  and incubated for additional 18 h or more (for the toxic oligomer stability assay).  $\text{A}\beta$  aggregation products were then separated using a 15% tris-tricine gel and stained using Imperial protein stain.

**Fluorescence Anisotropy Studies.** The appropriate inhibitor was dissolved in DMSO to a concentration of 50 nM and sonicated for 5 min. The solution was immediately mixed with aliquots of an  $\text{A}\beta_{1-42}$  intermediate (as described above) stock solution (20  $\mu\text{M}$ ) to varying final polypeptide concentrations. Polarization measurements were carried out using an ISS K2 fluorimeter. The solutions were excited at 280 nm and emission was monitored at 350 nm. For each single point, at least five measurements were collected and their average values were used for the calculation. All experiments were performed in phosphate-buffered saline, PBS [100 mM NaCl (pH 7.4)].

**$\text{IC}_{50}$  ThT Measurements.** Synthetic lyophilized  $\text{A}\beta_{1-42}$  was dissolved in DMSO to a concentration of 100  $\mu\text{M}$  and sonicated for 1 min to prevent preaggregation.  $\text{A}\beta$  solutions were prepared by immediate dilution with 10 mM PBS. The samples were again diluted to a final concentration of 5  $\mu\text{M}$  with the appropriate inhibitor concentration or with PBS for control samples. ThT fluorescence was measured after 24 h. The respective excitation and emission wavelengths were 450 nm (2.5 nm slit) and 480 nm (5 nm slit). A

10-fold diluted sample was taken and mixed with 900 mL of 0.4  $\mu\text{M}$  ThT. The fluorescence of ThT was measured using a Jobin Yvon Horiba Fluoromax 3 fluorimeter. Each experiment was repeated in quadruplicate.

**Fluorescence Screen for Inhibitors of  $\text{A}\beta$  Aggregation.** The vector for expressing the  $\text{A}\beta_{40}$ -GFP fusion was designed in the lab of Prof. Michael Hecht<sup>43</sup> and kindly given to us. *E. coli* cells harboring the  $\text{A}\beta_{40}$ -GFP fusion vector were grown in LB medium supplemented with 35  $\mu\text{g}/\text{mL}$  kanamycin. When cultures reached an  $\text{OD}_{600} = 0.8$ , 100  $\mu\text{L}$  of culture was transferred to the wells of 96-well plate. The compounds were added to each well, and protein expression was induced by adding isopropyl- $\beta$ -D-1-thiogalactopyranoside (IPTG) to a final concentration of 1 mM. Samples were incubated with gentle agitation at  $37^\circ\text{C}$ . Following 3 h of incubation, the fluorescence of each well was measured at 512 nm (excitation 490 nm) using an automated Synergy plate reader. To verify that cell densities were consistent across all samples, the  $\text{OD}_{600}$  was measured also at that point. Compounds were tested in quadruplicate for each compound concentration tested. The same protocol was conducted for  $\text{A}\beta_{42}$ -GFP fusion and the negative control (GFP alone).

## RESULTS

**Molecular Dynamics Simulations Show that Methylation at the Anilinic Nitrogen is Detrimental.** The *in silico* studies were performed on three amyloidogenic heptapeptides that span the central segment  $\text{A}\beta_{14-28}$ , which includes the aromatic side chains of Phe19 and Phe20. The choice of studying truncated constructs is motivated by two reasons. First, it is important to be able to obtain statistically reliable simulation results. Conformational transitions in the full-length  $\text{A}\beta_{40}$  or  $\text{A}\beta_{42}$  can occur on time scales that exceed the currently accessible regime,<sup>30</sup> while for the trimeric heptapeptide systems

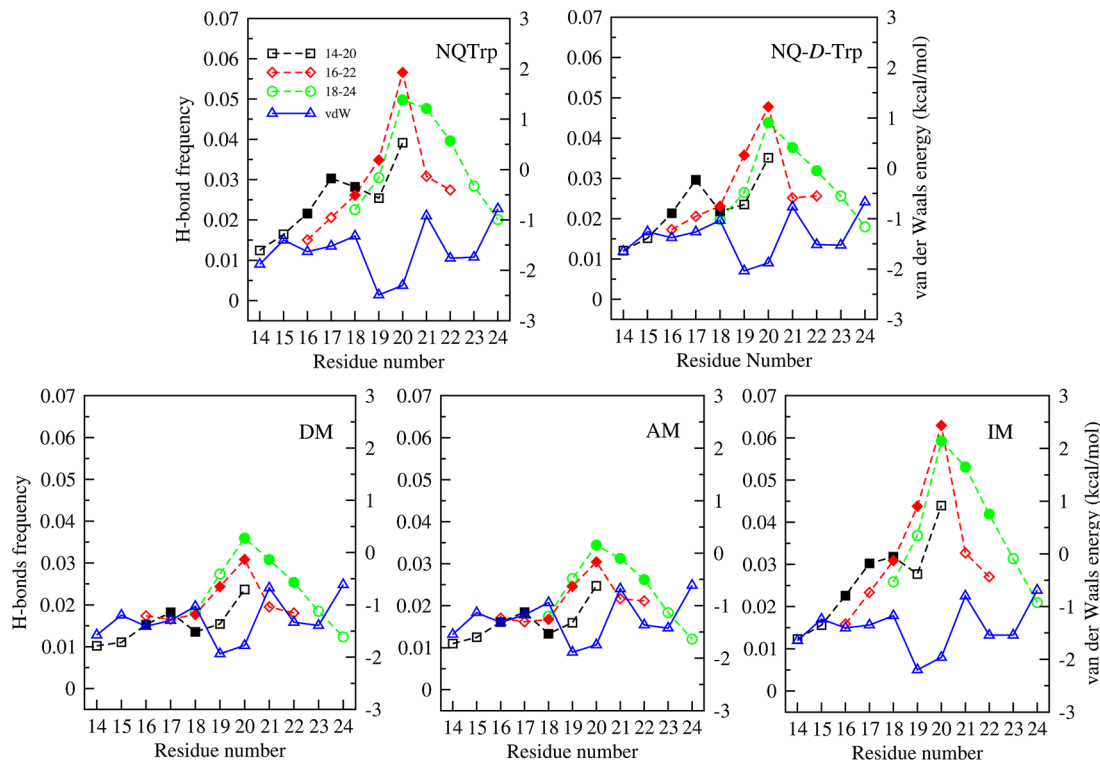


**Figure 2.** Interaction between NQTrp and its derivatives and  $\text{A}\beta$ . Frequency of interactions between all NQTrp and its derivatives CO groups and peptide backbone NHs (left y-axis). Open symbols correspond to residues proximal to the N-terminal or C-terminal of the peptide (positions 1, 2, 6, and 7 in each heptapeptide). Closed symbols correspond to the central residues (positions 3–5). Average van der Waals interaction energy between the residues and NQTrp are shown by blue triangles (right x-axis). Lower values correspond to more favorable interaction energy.

used here, convergence of the sampling was reached (see below and Figures S1 and S3 in the Supporting Information). Second, residues 14–24 highlight the role of the so-called central hydrophobic cluster,<sup>31</sup> residues L<sub>17</sub>VFFA<sub>21</sub>, which is often assumed to be critical in mediating peptide-inhibitor<sup>21</sup> as well as peptide–peptide interactions.<sup>32</sup> By discarding the hydrophobic C terminus, the present simulations focus on the possible specific roles played by the residues in this stretch. Neglecting the N-terminal region is justified by experimental<sup>33</sup> and simulation<sup>34</sup> studies that show this segment to be completely unstructured.

During the simulation the three investigated systems explore many different configurations, including aggregated, disaggregated,  $\beta$  structures with a variety of registers, and other spatial arrangements. The  $P_2$  order parameter (described in Materials and Methods) has been adopted to monitor the degree of orientational order within the oligomers: a value close to one corresponds to an ordered trimer, with either parallel or antiparallel  $\beta$ -sheet, while a value close to zero reflects a fully disordered system. The frequency histograms of  $P_2$  for the unperturbed and perturbed systems (Figure 1a) display a prominent peak at  $P_2 \sim 0.8$ , and a shoulder for  $P_2$  values lower than 0.5, which includes disordered aggregates and isolated peptides. The distribution of the interaction energy between peptide pairs (Figure 1b) shows two peaks. By visual inspection, and by comparing the pairwise interaction energies with the average  $P_2$  (blue line in Figure S1d in Supporting Information), the oligomeric structures can be assigned to the interaction energy distribution (see insets in Figure 1b). The peaks at -80 and -40 kcal/mol correspond to a peptide placed in the center and at the edge of an ordered trimer, respectively, irrespective of the heptapeptide. The comparison with the free

system (dashed line, Figure 1) reveals that the simulations in the presence of NQTrp or its derivatives have more events with pairwise interaction energy close to zero, originating mainly from disordered trimers. Notably, the trimeric state is predominant in all of the simulations (Figure S2 in Supporting Information). The presence of NQTrp or its derivatives does not enhance the statistical weight of the monomeric state; it rather causes an increased frequency of disordered trimers as well as dimers. This is due to the ability of polycyclic aromatic moieties to intercalate between aggregated  $\text{A}\beta$  peptides and establish an intermolecular hydrogen bond network and, thus, destabilize their organized structure<sup>35</sup> without a total rupture of the trimer.

The inhibitors studied here have a small but relevant effect on the equilibrium properties of the unperturbed oligomeric system. Coarse-grained simulations have shown that even a small perturbation of the polypeptide free energy landscape, for example, destabilization of the aggregation-prone state by only 1 kcal/mol, significantly influences the kinetics and the thermodynamics of the aggregation process.<sup>36</sup> These simulation results could explain why a small perturbation produces the macroscopic decrease of amyloid aggregation observed experimentally in presence of inhibiting compounds.

The overall ability of the NQTrp or its derivatives to alter the order/disorder ratio of the three heptapeptides can be quantified by the parameter  $r$ , which is calculated using the nematic order parameter  $P_2$  (see Materials and Methods). Interestingly, the presence of NQTrp, NQ-D-Trp and IM results in a higher disorder than DM and AM irrespective of the heptapeptide segment (Table 2). Note that the heptapeptide segment  $\text{A}\beta_{14-20}$  has a much stronger tendency to form parallel  $\beta$ -sheets than the segments  $\text{A}\beta_{16-22}$  or  $\text{A}\beta_{18-24}$  (Table 2).

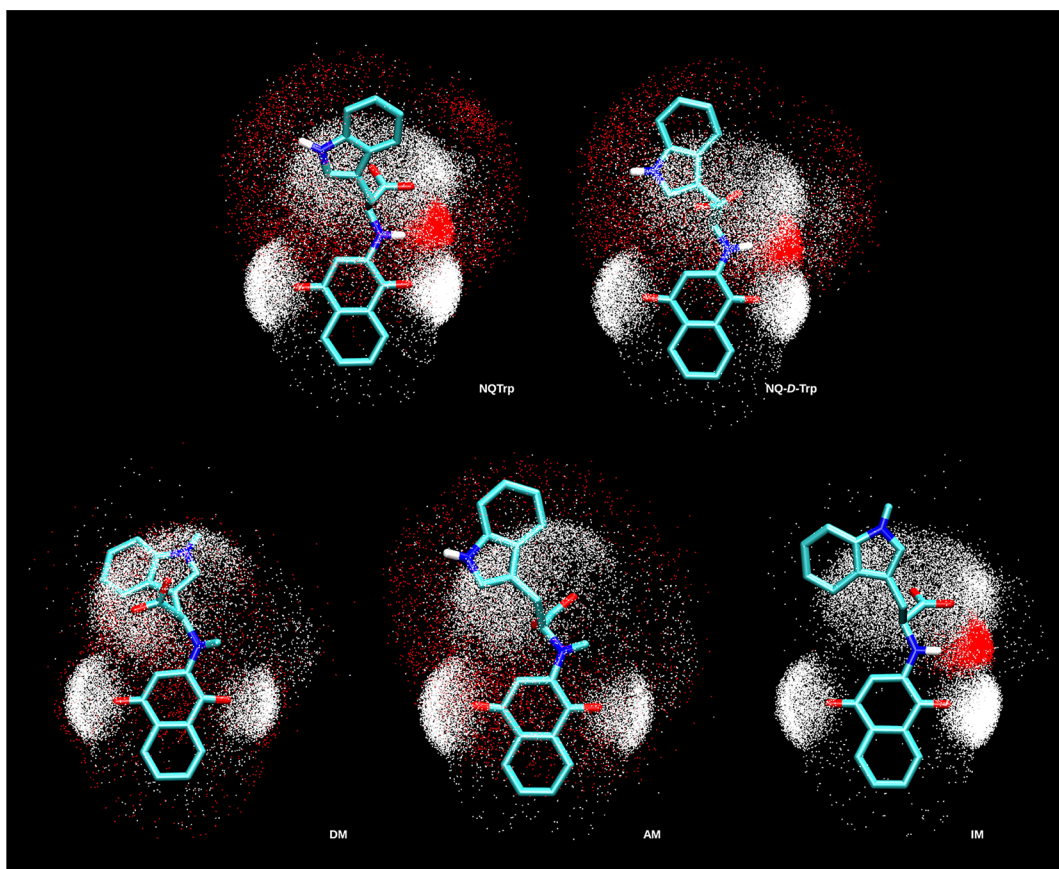


**Figure 3.** Interactions between  $\text{A}\beta$  backbone polar groups and investigated molecules. The position of backbone carbonyl oxygens and amide hydrogens that are within 2.5 Å from any atom in NQTrp and its derivatives are shown by dots to display the corresponding coordination. Denser clouds indicate a volume with higher coordination.

The detrimental effect of the methylation of the anilinic nitrogen (in DM and AM) is consistent with the involvement of the anilinic NH of NQTrp in hydrogen bonds (HBs) with the peptide backbone carbonyls of residues 20 and 21 of  $\text{A}\beta$  as reported previously.<sup>27</sup> Analysis of the peptide HBs shows that each of the compounds increases the number of intrapeptide HBs at the expenses of the interpeptide HBs (Table 2). In other words, all compounds are able to reduce the cross- $\beta$  interactions, thereby increasing the propensity of the individual heptapeptides to form intrachain contacts/hydrogen bonds. In agreement with the order/disorder ratio, the reduction of interpeptide HBs is less pronounced for the two derivatives with methylated anilinic nitrogen, that is, AM and DM, irrespective of the heptapeptide segment.

The distribution of interpeptide interaction energy is influenced by each of the five NQTrp-derived compounds. The main effect is a shift toward less favorable values (i.e., toward zero) in the presence of any of the compounds, with a decrease of the frequency at the peak corresponding to the central peptide in the three-stranded  $\beta$ -sheet (at about -80 kcal/mol in Figure 1b), which ranges from 11 to 20% for  $\text{A}\beta_{14-20}$ , from 22 to 35% for  $\text{A}\beta_{16-22}$ , and from 27 to 38% for  $\text{A}\beta_{18-24}$ . The same effect is observed at the peak corresponding to the lateral strands (at about -40 kcal/mol, Figure 1b), with a decrease of frequency ranging from 45 to 50% for  $\text{A}\beta_{14-20}$ , from 20 to 40% for  $\text{A}\beta_{16-22}$ , and from 20 to 40% for  $\text{A}\beta_{18-24}$ . The profile along the  $\text{A}\beta_{14-28}$  sequence of the intermolecular van der Waals energy is similar for different compounds (Figure 2, blue solid line). It shows that the most favorable van der Waals

interaction is with Phe19 followed by Phe20 irrespective of the type of NQTrp derivative. In agreement with the aforementioned analysis of order/disorder and peptide HBs, the DM and AM derivatives show less favorable van der Waals energy with  $\text{A}\beta_{14-28}$  than NQTrp, NQ-D-Trp, and IM. More specifically, for the DM and AM derivatives there is a less favorable van der Waals interactions with Phe19 and Phe20 (-1.9 kcal/mol and -1.7 kcal/mol, respectively) than NQTrp, NQ-D-Trp, and IM (-2.3 kcal/mol and -2.0 kcal/mol with Phe19 and Phe20, respectively). In addition, the profile of the frequency of hydrogen bonds between any oxygen atom of the compound and the backbone NH groups of  $\text{A}\beta_{14-28}$  (dashed lines in Figure 2) shows a peak at the NH of Phe20 which is again less pronounced for the two derivatives with methylated anilinic nitrogen.

The present simulation results on the NQTrp derivatives provide additional evidence for the main interactions between NQTrp and  $\text{A}\beta$  as reported previously.<sup>27</sup> Briefly, NQTrp can assume a relatively compact conformation in which the indole and naphthoquinone double-ring systems "clamp" the phenyl rings of Phe19 or Phe20 (see Figures 7A–C of ref 27). New information on the effect of methylation of the hydrogen bond donor is obtained in the present study. Methylation of the anilinic NH group of the NQTrp derivatives reduces the possibility of establishing a pattern of hydrogen bonds involving also the carbonylic and the carboxylic CO group. This observation emerges from the comparative analysis of the coordination cloud of the  $\text{A}\beta$  backbone atoms around NQTrp and its derivatives (Figure 3). It is evident that NQTrp and

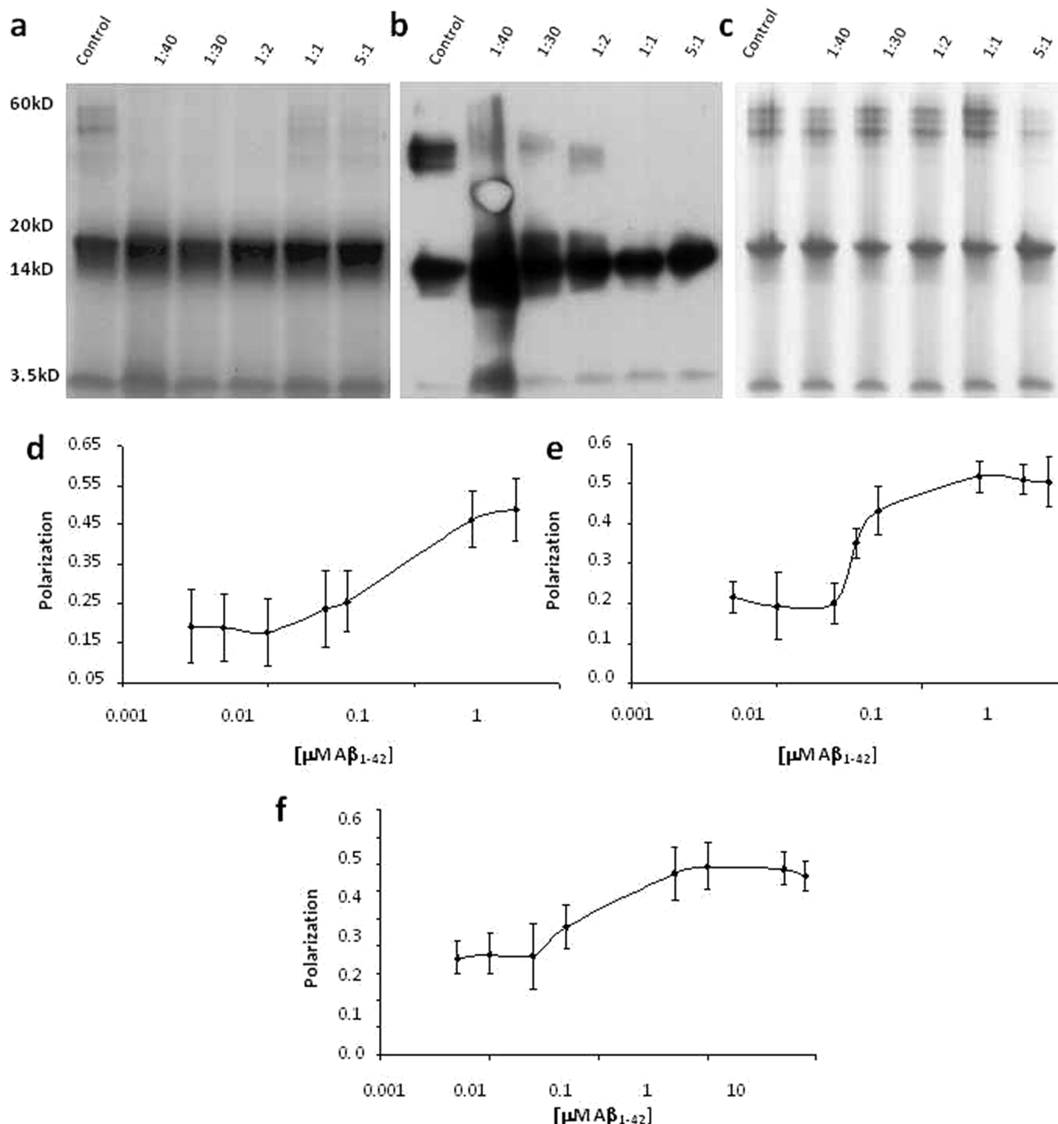


**Figure 4.**  $\text{A}\beta$  oligomer inhibition by three derivatives of NQTrp. Determination of the dose-dependent effect of (a) NQ-D-Trp, (b) IM, and (c) AM on soluble oligomer formation. Soluble oligomers were prepared with and without increasing concentration of the compounds.  $\text{A}\beta$  concentration was set at 133  $\mu\text{M}$ . Molar ratios of  $\text{A}\beta$ : NQTrp derivative are indicated. (d–f) Anisotropy analysis of three NQTrp derivatives. The affinity of the compounds toward early oligomers was determined using fluorescence anisotropy. (d) NQ-D-Trp, (e) IM, and (f) AM.

NQ-D-Trp are characterized by the presence of  $\text{A}\beta$  backbone NH clouds (white dots) around their carbonyl and carboxyl oxygens, and  $\text{A}\beta$  backbone oxygen clouds (red dots) around their indolic and anilinic NH groups. The coordination cloud is reduced in DM and AM in which the anilinic nitrogen methylation not only zeroes the oxygen coordination around the anilinic NH but also significantly reduces the hydrogen coordination clouds around the carbonyl and carboxyl oxygens. On the other hand, the coordination clouds are not affected by the difference in stereochemistry NQTrp versus NQ-D-Trp, and only locally influenced by the methylation of the indolic nitrogen in IM, as shown by the reduction of the  $\text{A}\beta$  backbone oxygen cloud (red dots) only around the indolic ring of IM.

**Oligomer Inhibition.** Following the in silico work we examined its prediction by in vitro assays. The inhibitory effect of the NQTrp derivatives was analyzed by incubating various concentrations of the compounds with monomers of synthetic  $\text{A}\beta_{1-42}$  following the protocol Barghorn and co-workers.<sup>10</sup> This protocol results in the formation of SDS-stable oligomers that

display toxic effects on the long-term potentiation of cultured neural cells. The reaction mixtures were then resolved on SDS-PAGE. Only three of the four derivatives were analyzed: NQ-D-Trp, AM, and IM, the fourth compound, the DM was not analyzed due to synthesis problems as stated above. The three derivatives differed in their inhibitory potential toward formation of the  $\text{A}\beta$  56kD species (Figure 4a–c). Previously we have reported that increasing concentrations of NQTrp results in marked reduction of 56kD oligomers and accumulation of smaller 18kD oligomers, which are known to be nontoxic<sup>10,27</sup> this can also be seen for the NQ-D-Trp and IM compounds, though no such reduction is observed for the AM compound.

**Interaction between the NQTrp Derivatives and  $\text{A}\beta$  Oligomers.** We next evaluated the affinity of the NQTrp derivatives toward  $\text{A}\beta$  oligomers.  $K_d$  was measured by tryptophan anisotropy (Figure 4d–f, Table 3) based on the intrinsic fluorescence of the Trp-substituted quinones and their relatively small size as compared to the  $\text{A}\beta$  oligomers.

**Table 3. Summary of the Derivatives  $K_d$ ,  $IC_{50}$  towards Fibrillation and Log P Estimation (DAIM)**

	$K_d$ toward oligomers	$IC_{50}$ toward fibrillation	log P estimation (DAIM)
NQTrp	90 nM	10–100 nM	4.48
NQ-D-Trp	90 nM	5–10 nM	4.48
DM			5.9
AM	250 nM	25–50 mM	5.19
IM	90 nM	50 mM	5.9

Increasing concentrations of early assemblies of  $A\beta_{1-42}$  were titrated into a solution of the appropriate tested compound and anisotropy was determined (Figure 4d–f). The results indicate that the affinity of both NQ-D-Trp and IM toward  $A\beta$  oligomers is similar to that of the parent compound NQTrp, while the  $K_d$  of the AM compound is higher, suggesting lower binding and affinity toward  $A\beta$ .

**Inhibition of  $A\beta$  Amyloid Fibril Formation by the NQTrp Derivatives.** We next examined whether the derivatives are able to inhibit the formation of the mature  $A\beta$  fibrils using the thioflavin-T binding assay.  $A\beta_{1-42}$  was allowed to form amyloid fibrils either in the absence or in the presence of increasing concentrations of the appropriate derivative (Figure 5a). The process of fibrillization was followed for 270 h. By this time a plateau of fluorescence values was reached which corresponds to a plateau in  $A\beta$  fibril growth. The fluorescence values were recorded at 270 h and the corresponding  $IC_{50}$ s were calculated (Table 3). The results show that NQ-D-Trp has an  $IC_{50}$  (5–10 nM) that is even lower than the original NQTrp (10–100 nM) molecule, whereas both methylated derivatives (AM and IM) exhibit a higher  $IC_{50}$  value toward  $A\beta$  fibrils (AM = 25–50  $\mu$ M, IM = 50  $\mu$ M).

**Inhibition of Aggregation of Bacterially Expressed  $A\beta_{1-42}$  Fused to GFP.** To corroborate the in vitro results we examined the inhibitory effect of the various compounds tested toward aggregation of GFP-  $A\beta_{1-42}$  expressed in *E. coli*<sup>37</sup> (kindly provided by Prof. Michael Hecht, Princeton University). Low fluorescence of the GFP protein corresponds to a highly aggregated  $A\beta$  peptide, whereas high fluorescence is directly proportional to reduced  $A\beta$  aggregation (Figure 5b). The results of this assay show that NQTrp, NQ-D-Trp, and IM increase GFP fluorescence compared to  $A\beta_{1-42}$  without any compound, indicating decrease in  $A\beta$  aggregation, while no increase in fluorescence was apparent for the AM compound indicating a lower inhibitory potential.

## CONCLUSIONS

Four derivatives of NQTrp were designed. In three of them, the structural elements, which were previously shown to be essential for NQTrp binding, were blocked by methyl groups. In the third derivative, the Trp amino acid was modified from L to D. We wanted to analyze the effect of these changes on the amyloid inhibition potential of NQTrp. The in silico results suggest that NQTrp, NQ-D-Trp, and IM have a comparable inhibitory activity toward the early oligomerization as well as a comparable molecular affinity toward the oligomer of  $A\beta$ , while DM and AM are less inhibitory and have lower affinity. The methylation of the anilinic nitrogen abolishes the inhibitory activity and affinity toward  $A\beta$  oligomers. This confirms the initial hypothesis of the importance of the hydrogen bond pattern formed by naphthoquinonic carbonyls, anilinic nitrogen and the carboxyl group of NQTrp and NQ-D-Trp with the  $A\beta$

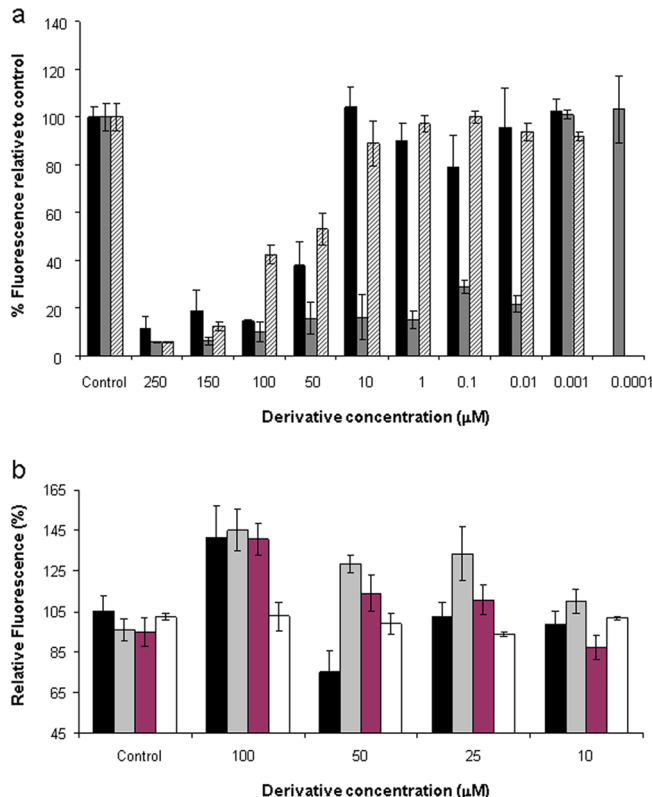


**Figure 5.** (a) ThT fluorescence assay of three derivatives of NQTrp.  $A\beta_{1-42}$  was incubated alone or with increasing concentrations of each of the four compounds and the fluorescence was measured after 72 h. The inhibition is shown relative to  $A\beta$  alone which is shown as 100% fluorescence (black bars, AM-NQTrp; gray bars, NQ-D-Trp; dashed line bars, IM-NQTrp). (b) Inhibition of aggregation of bacterially expressed  $A\beta_{1-42}$  fused to GFP: The fluorescence of GFP was measured with and without increasing concentrations of the four analyzed compounds. The % fluorescence is shown relative to  $A\beta_{1-42}$  without compounds (black bars, IM-NQTrp; gray bars, NQ-D-Trp; white bars, AM-NQTrp; pink bars, NQTrp).

peptide backbone.<sup>27</sup> The methylation of the indolic nitrogen, as well as the stereochemistry of the compound, do not seem relevant neither for the inhibition activity of the oligomerization nor for the affinity toward the  $A\beta$  oligomer. However, the modifications examined seem to have a different effect on the inhibitory activity toward  $A\beta$  fibrillization. According to the experimental data in Table 3, IM shows reduced inhibition of  $A\beta$  fibrillization while showing no reduced inhibitory effect toward  $A\beta$  oligomers as well as having the same affinity constant toward the oligomers as does the parent compound NQTrp. This probably reflects a higher solubility of NQTrp and NQ-D-Trp resulting in increased fibrillation inhibitory activity. Methylation of the compound at the indole ring makes this molecule more hydrophobic and less soluble in the PBS buffer used for analysis of fibril formation. On the other hand, as expected,<sup>27</sup> the AM derivative does in fact show reduced inhibition potential both toward the fibrillization and the oligomerization of  $A\beta$  (Table 3 and Figures 4 and 5a), as verified both by its higher  $K_d$  and  $IC_{50}$  as compared to the parent NQTrp molecule (Table 3). The reduced inhibitory potential of AM toward fibrillation of  $A\beta$  can also result from its reduced solubility in the PBS buffer due to the methylation of the hydrogen bond. However, in the oligomer assay there is less of a solubility problem because a higher percent of DMSO (in

PBS) is used (8% DMSO as compared to 1% DMSO in the fibril assay). The solubility of both IM and AM increases at higher DMSO percentages. As shown in the in silico analysis and previously proposed,<sup>27</sup> the hydrogen bond formed between A $\beta$  and the anilinic position of NQTrp is crucial both for binding A $\beta$  and for inhibiting its aggregation. Presently, no experimental data is available for DM. Thus, we cannot completely exclude the importance of a variation of physical-chemical property, for example, solubility of all the compounds, in the fibril inhibition assays (see Table 3). NQTrp and NQ-D-Trp have an estimated log P (computed with the in-house developed software DAIM) lower than IM.<sup>38</sup>

Taken together, the simulation and experimental results indicate the following: (1) Stereochemistry of the Trp C $\alpha$  is not important for obtaining inhibitory activity toward the oligomerization of A $\beta$ ; (2) The methylation of the indole nitrogen does not affect the affinity toward the oligomers but the inhibitory activity toward fibrillization is reduced; (3) The methylation of the anilinic nitrogen reduces the hydrogen bond frequency but does not affect the van der Waals interaction energy with all peptide residues. This can reduce the affinity ( $K_d$ ) toward oligomers and cause reduction in the fibrillization inhibitory activity; (4) The interactions with Phe19 and Phe20 are important for all five investigated compounds; (5) AM shows lower affinity ( $K_d$ ) for the oligomers than IM, NQ-D-Trp and their parent compound NQTrp; (6) The predicted rank of the molecules according to their inhibitory activity toward fibrillization and/or oligomerization is NQTrp  $\approx$  NQ-D-Trp > IM  $\gg$  AM  $\geq$  DM; (7) This is further confirmed experimentally (with the exception of DM).

## ■ ASSOCIATED CONTENT

### Supporting Information

Additional supporting figures. This material is available free of charge via the Internet at <http://pubs.acs.org>.

## ■ AUTHOR INFORMATION

### Author Contributions

<sup>†</sup>These authors contributed equally to this work.

### Notes

The authors declare no competing financial interest.

## ■ ACKNOWLEDGMENTS

This work was supported in part by grants from the Israeli Ministry of Health, Parkinson's Disease Foundation, Colton Foundation, and the Lord Alliance Family Trust. The work carried out at the University of Zurich was supported by a grant of the Swiss National Science Foundation to A.C.

## ■ REFERENCES

- (1) Brookmeyer, R.; Johnson, E.; Ziegler-Graham, K.; Arrighi, H. M *Alzheimer's Dementia* **2007**, *3*, 186–191.
- (2) Bharadwaj, P. R.; Dubey, A. K.; Masters, C. L.; Martins, R. N.; Macreadie, I. G. *J. Cell. Mol. Med.* **2009**, *13*, 412–421.
- (3) Bertram, L.; Lill, C. M.; Tanzi, R. E. *Neuron* **2010**, *68*, 270–281.
- (4) Selkoe, D. J. *Neuro* **1991**, *487–498*.
- (5) Terry, R. *Prog. Brain Res.* **1994**, *383–390*.
- (6) Kirkpatridge, M. D.; Bitan, G.; Teplow, D. B. *J. Neurosci. Res.* **2002**, *567–577*.
- (7) Lashuel, H. A.; Hartley, D.; Petre, B. M.; Walz, T.; Lansbury, P. T. J. *Nature* **2002**, *291*.
- (8) Kayed, R.; Head, E.; Thompson, J. I.; McIntire, T. M.; Milton, S. C.; Cotman, V. W.; Glabe, C. G. *Science* **2003**, *300*, 486–489.
- (9) Gazit, E. *Drugs Future* **2004**, *29*, 613–619.
- (10) Barghorn, S.; Nimmrich, V.; Striebinger, A.; Krantz, C.; Keller, P. B. J.; Bahr, M.; Schmidt, M.; Bitner, R. S.; Harlan, J.; Barlow, E.; Ebert, U.; Hillen, H. *J. Neurochem.* **2005**, *95*, 834–847.
- (11) Azriel, R.; Gazit, E. *J. Biol. Chem.* **2001**, *276*, 34156–34161.
- (12) Gazit, E. *FASEB J.* **2002**, *16*, 77–83.
- (13) Gazit, E. *Bioinformatics* **2002**, *880–883*.
- (14) Jacobsen, J. S.; Wu, C. C.; Redwine, J. M.; Comery, T. A.; Arias, R.; Bowlby, M.; Martone, R.; Morrison, J. H.; Pangalos, M. N.; Reinhart, P. H.; Bloom, F. E. *Proc. Natl. Acad. Sci. U.S.A.* **2006**, *5161–5166*.
- (15) Porat, Y.; Kolusheva, S.; Jelinek, R.; Gazit, E. *Biochemistry* **2003**, *10971–10977*.
- (16) Mazor, Y.; Gilead, S.; Benhar, I.; Gazit, E. *J. Mol. Biol.* **2002**, *1013–1024*.
- (17) Reches, M.; Gazit, E. *Science* **2003**, *625–627*.
- (18) Reches, M.; Gazit, E. *Amyloid* **2004**, *81–89*.
- (19) Cohen, T.; Frydman-Marom, A.; Rechter, M.; Gazit, E. *Biochemistry* **2006**, *45*, 4727–4735.
- (20) Makin, O. S.; Atkins, E.; Sikorski, P.; Johansson, J.; Serpell, L. C. *M. Proc. Natl. Acad. Sci. U.S.A.* **2005**, *102*, 315–320.
- (21) Porat, Y.; Abramowitz, A.; Gazit, E. *Chem. Biol. Drug Des.* **2006**, *27–37*.
- (22) Hamaguchi, T.; Ono, K.; Yamada, M. *Cell. Mol. Life Sci.* **2006**, *1538–1552*.
- (23) Lorenzo, A.; Yankner, B. A. *Proc. Natl. Acad. Sci. U.S.A.* **1994**, *91*, *12243–12247*.
- (24) Lee, V. M. *Neurobiol. Aging* **2002**, *23*, *1039–1042*.
- (25) Poli, G.; Ponti, W.; Carcassola, G.; Ceciliani, F.; Colombo, L.; Dall'Ara, P.; Gervasoni, M.; Giannino, M. L.; Martino, P. A.; Pollera, C.; Villa, S.; Salmona, M. *Arzneimittelforschung* **2003**, *53*, *875–888*.
- (26) Scherzer-Attali, R.; Shaltiel-Karyo, R.; Adalist, Y. H.; Segal, D.; Gazit, E. *Proteins* **2012**, *80*, *1962–1973*.
- (27) Scherzer-Attali, R.; Pellarin, R.; Convertino, M.; Frydman-Marom, A.; Egoz-Matia, N.; Peled, S.; Levy-Sakin, M.; Shalev, D. E.; Caflisch, A.; Gazit, E.; Segal, D. *PLoS One* **2010**, *5*, e11101.
- (28) Chebaro, Y.; Jiang, P.; Zang, T.; Mu, Y.; Nguyen, P. H.; Mousseau, N.; Derreumaux, P. *J. Phys. Chem. B* **2012**, *116*, *8412–8422*.
- (29) Convertino, M.; Vitalis, A.; Caflisch, A. *J. Biol. Chem.* **2011**, *286*, *41578–41588*.
- (30) Straub, J. E.; Guevara, J.; Huo, S.; Lee, J. P. *Acc. Chem. Res.* **2002**, *35*, *473–481*.
- (31) Zhang, S.; Casey, N.; Lee, J. P. *Fold. Des.* **1998**, *3*, *413–422*.
- (32) Tjernberg, L. O.; Naslund, J.; Lindqvist, F.; Johansson, J.; Karlstrom, A. R.; Thyberg, J.; Terenius, L.; Nordstedt, C. *J. Biol. Chem.* **1996**, *271*, *8545–8548*.
- (33) Williams, A. D.; Portelius, E.; Kheterpal, I.; Guo, J. T.; Cook, K. D.; Xu, Y.; Wetzel, R. *J. Mol. Biol.* **2004**, *335*, *833–842*.
- (34) Vitalis, A.; Caflisch, A. *J. Mol. Biol.* **2010**, *403*, *148–165*.
- (35) Convertino, M.; Pellarin, R.; Catto, M.; Carotti, A.; Caflisch, A. *Protein Sci.* **2009**, *18*, *792–800*.
- (36) Pellarin, R.; Caflisch, A. *J. Mol. Biol.* **2006**, *360*, *882–892*.
- (37) Wurth, C.; Guimard, N. K.; Hecht, M. H. *J. Mol. Biol.* **2002**, *319*, *1279–1290*.
- (38) Kolb, P.; Caflisch, A. *J. Med. Chem.* **2006**, *49*, *7384–7392*.
- (39) Shrestha-Dawadi, P. B.; Prativa, B.; Bittner, S.; Fridkin, M.; Rahimipour, S. *Synthesis* **1996**, *1468–1472*.
- (40) Bassindale, A. R.; Parker, D. J.; Patel, P.; Taylor, P. G. *Tetrahedron Lett.* **2000**, *41*, *4933–4936*.
- (41) Brooks, B. R.; Brooks, C. L.; Mackerell, A. D.; Nilsson, L.; Petrella, R. J.; Roux, B.; Won, Y.; Archontis, G.; Bartels, C.; Boresch, S.; Caflisch, A.; Caves, L.; Cui, Q.; Dinner, A. R.; Feig, M.; Fischer, S.; Gao, J.; Hodoscek, M.; Im, W.; Kuczera, K.; Lazaridis, T.; Ma, J.; Ovchinnikov, V.; Paci, E.; Pastor, R. W.; Post, C. B.; Pu, J. Z.; Schaefer, M.; Tidor, B.; Venable, R. M.; Woodcock, H. L.; Wu, X.; Yang, W.; York, D. M.; Karplus, M. *J. Comput. Chem.* **2009**, *30*, *1545–1614*.
- (42) Ferrara, P.; Apostolakis, J.; Caflisch, A. *Proteins Struct. Funct. Bioinf.* **2002**, *46*, *24–33*.

(43) Kim, W.; Kim, Y.; Min, J.; Kim, D. J.; Chang, Y. T.; Hecht, M. H. *ACS Chem. Biol.* **2006**, *1*, 461–469.